RESEARCH ON DYNAMIC RESPONSES AND RESIDUAL STRESSES FIELDS INDUCED BY LSP IN DD6 ALLOY BLADE

Y.W. FANG†, L.W. YANG, S.H.. ZHAO, Y. WANG and X.S. GAN

† *Information and Navigation College, Air Force Engineering University, Xi'an 710077, PR China.*
fangyw72@126.com

***Abstract*— The aim of this article was to address the dynamic responses properties and the residual stresses fields induced by laser shock processing (LSP) in a DD6 alloy blade. The dynamic characteristics with [001] and [111] orientations were investigated under different rotor speeds and temperatures by finite element method (FEM) simulation and vibration experiment. As a result, the corresponding static frequencies were analyzed for different temperature, rotor speed and orientation. The residual stresses fields induced by LSP were addressed for [001] orientation at 980^{0}C based on simulation and LSP experiment. Results shown the proposed model was effective. The analyses indicate that the trends of different orders static frequencies were same along [001] and [111], and the orientation had stronger effect on high order static frequencies than it had on low order ones. The best compressive residual stress was achieved to be about 600 MPa when the power density was 4.5 GPa.**

***Keywords*— Dynamic properties; Laser shock processing; Residual stresses fields; DD6 alloy blade**

I. INTRODUCTION

Ghosh and Mclean gave modeling process of the tertiary creep of single crystal superalloy along different orientation (Ghosh and Mclean, 1989). Wasson and Fuchs (2008) investigated the effect of carbide morphologies on elevated temperature tensile and fatigue behavior of a modified nickel-based single crystal superalloy. He *et al*. (2002) discussed the creep/fatigue damage characteristics and of DD6 materials at high temperature by FEM, and the results show the capability of DD6 to avoid fatigue damages in [011] direction is better than that in [001] direction. Shi *et al.* (2011) and Li *et al.* (2005) detailed analyzed the high/low cycle fatigue behaviors of the nickel-based single crystal superalloy DD6 by experiment. At the same time, Amarchinta1 *et al*. (2009) and Wu *et al*. (2010) discussed the dynamic characteristics of aluminum alloy and stainless steel during LSP process by simulation and experiment. Zhang *et al*. (2009) and Fang *et al*. (2011) analyzed in detail the effects of LSP on the residual stresses and stress corrosion of some common materials by experiments. Present researches show compressive residual stresses have very important merits for improving the fatigue life of materials. But the related studies are still insufficient in DD6 alloy blade. In order to attain an excellent surface treatment purpose, it is very necessary to investigate dynamic responses properties and residual stresses fields induced by LSP in a DD6 alloy blade.

II. DYNAMIC MODELING

According to combined flow rule, the plastic constitutive relation can be expressed by isotropic hard model based on the elastic- plastic relations.

$$d\varepsilon_{ij}^{p} = \frac{1}{H'}\frac{\partial\overline{\sigma}}{\partial\sigma_{ij}}d\overline{\sigma}, \tag{1}$$

$$d\varepsilon_{ij}^{p} = \frac{\partial\overline{\sigma}}{\partial\sigma_{ij}}d\overline{\varepsilon}_{p}, \tag{2}$$

where H' is the isotropic hardening modulus, $\partial\overline{\sigma}/\partial\sigma_{ij}$ can be gotten.

The following equations can be obtained

$$\begin{aligned} d\overline{\sigma} &= \frac{\partial\overline{\sigma}}{\partial\sigma_{11}}d\sigma_{11} + \frac{\partial\overline{\sigma}}{\partial\sigma_{22}}d\sigma_{22} + \frac{\partial\overline{\sigma}}{\partial\sigma_{33}}d\sigma_{33} \\ &+ \frac{\partial\overline{\sigma}}{\partial\sigma_{23}}d\sigma_{23} + \frac{\partial\overline{\sigma}}{\partial\sigma_{31}}d\sigma_{31} + \frac{\partial\overline{\sigma}}{\partial\sigma_{12}}d\sigma_{12} = \left\{\frac{\partial\overline{\sigma}}{\partial\sigma}\right\}^{T} d\{\sigma\} \end{aligned}, \tag{3}$$

$$d\{\sigma\} = [S]^{-1}\left(d\{\varepsilon\} - d\{\varepsilon_{p}\}\right). \tag{4}$$

Left multiplication $\{\partial\overline{\sigma}/\partial\sigma\}^{T}$ to the Eq. (4) results in

$$\left\{\frac{\partial\overline{\sigma}}{\partial\sigma}\right\}^{T} d\{\sigma\} = \left\{\frac{\partial\overline{\sigma}}{\partial\sigma}\right\}^{T}[S]^{-1}\left(d\{\varepsilon\} - d\{\varepsilon_{p}\}\right). \tag{5}$$

Finally, the elastic-plastic matrix can be obtained

$$[C]_{ep} = [S]^{-1} - \frac{[S]^{-1}\left\{\frac{\partial\overline{\sigma}}{\partial\sigma}\right\}\left\{\frac{\partial\overline{\sigma}}{\partial\sigma}\right\}^{T}[S]^{-1}}{H' + \left\{\frac{\partial\overline{\sigma}}{\partial\sigma}\right\}^{T}[S]^{-1}\left\{\frac{\partial\overline{\sigma}}{\partial\sigma}\right\}}, \tag{6}$$

Based on the crystal plasticity theory, a explicit expression of elastic-plastic matrix $[C]_{ep}$ can be educed based on the related literature (Meric *et al*. 1991).

The natural frequencies of DD6 blade can be calculated by the following equation, and the modal shapes of DD6 blade can be gotten easily.

$$\begin{aligned} &\sum \iiint_{e} ([B]^{e})^{T}[C]_{ep}[B]^{e}\,dv\{X\} \\ &= \omega \sum \rho \iiint_{e} [V]^{T}[N]dv\{X\} \end{aligned}. \tag{7}$$

Assuming that the yielding occurs when the stress in the direction of the wave propagation reaches the *HEL*, the dynamic yield strength δ_y^D under uniaxial strain conditions can be defined in terms of the *HEL* by (Rubio-González *et al*., 2011)

$$\delta_y^D = HEL\frac{1-2\nu}{1-\nu}, \tag{8}$$

where υ represents Poisson's ratio.

When simulating residual stresses in the DD6 blade induced by LSP, the models of shock pressure and material model must be established. In this research, the Fabbro model and Johnson-Cook (JC) model were used to calculating LSP (Johnson and William, 1985).

$$P = 0.01\sqrt{\frac{ZAI_0\alpha}{2\alpha+3}}, \tag{9}$$

$$\sigma_y = \left(A + B\varepsilon^n\right)\left(1 + C\ln\varepsilon^*\right)\left(1-\left(T^*\right)^m\right), \tag{10}$$

where α denotes the efficiency coefficient, A denotes the absorbing facto, I_0 denotes the laser power density, and Z denotes the equivalent impedance. σ_y denotes the effective stress, A, B, C and m denote the material constants, n denotes the work hardening exponent, and ε^* denotes the non-dimensional plastic strain rate.

At last, the dynamic responses properties of a DD6 blade with different orientation, rotor speed and temperature could be calculated by the procedure proposed. As a result, LS-DYNA and ANSYS could be chosen to accomplish full FEM simulation during multiple LSP.

III. NUMERICAL SIMULATION AND EXPERIMENT

A. FEM Model

A case of a certain type of DD6 blade was simulated to analyze the dynamic response properties and residual stresses fields induced by LSP. The FEM model of a DD6 alloy blade was established as shown in Fig. 1. In order to improve the calculated precision, the tetrahedral element of twenty nodes was adopted in the DD6 blade except the rabbet, and solid 164 explicit elements were used to the FEM model.

Owing to the dovetail of the DD6 blade was fixed to compressor, the bottom of rabbet was assumed as the full constraint. In order to efficient investigate the effect of different temperature, orientation and rotor speed to the dynamic responses properties, the orientations of [001] and [111], the temperatures of 760^{0}C, 980^{0}C and 1070^{0}C, and the rotor speeds of 600r/s and 800r/s were selected to simulate the dynamic responses properties in the DD6 alloy blade according to the given conditions and parameters. On the basis of this research, the corresponding residual stresses fields were addressed.

Fig.1. FEM model of a DD6 blade

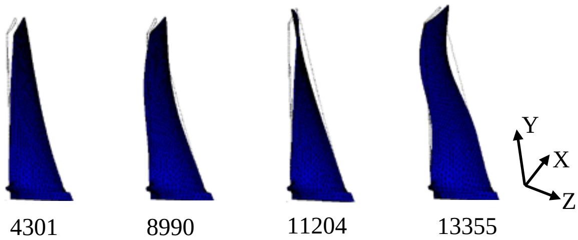

Fig. 2 The first four modal shapes of [001] orientation at 980^{0}C

B. Dynamic Responses Properties

In this section, the dynamic responses properties of [001] and [111] with different temperatures were analyzed mainly. At last, and the static frequencies and modal shapes of DD6 alloy blade were gotten, and the first four modal shapes of [001] orientation at 980^{0}C were also shown in Fig.2. The first five static frequencies of [001] and [111] orientations at 760^{0}C, 980^{0}C and 1070^{0}C were calculated, as presented in Table 1. Comparison of the computational and experimental results for different temperature and orientation was also obtained, as shown in Fig.3.

It was seen from Fig.3 that the static frequencies of [001] orientation was smaller than that of [111] when the temperature was same, and the maximum difference between the computational and experimental values was 15.8% along [111] orientation at 1070^{0}C. The values of static frequency were decreased along [001] and [111] orientations with the elevated temperature, the trends of

Table 1 The first five static frequencies

Orientation	Temperature (0C)	The first five static frequencies(Hz)					
		Computational values	4912	9308	12196	14088	16751
	760	Experimental values	4878	8579	11148	12691	14916
		Relative error (%)	7.0	8.5	9.4	11	12.3
		Computational values	4301	8990	11204	13355	16008
[001]	980	Experimental values	4005	8233	10121	11903	14067
		Relative error (%)	7.4	9.2	10.7	12.2	13.8
		Computational values	4075	8123	10096	12113	15264
	1070	Experimental values	3722	7305	8966	10625	13227
		Relative error (%)	9.5	11.2	12.6	14.0	15.4
		Computational values	5310	10412	13328	13548	16943
	760	Experimental values	4908	9517	12018	11979	14810
		Relative error (%)	8.2	9.4	10.9	13.1	4.4
		Computational values	5190	9987	12209	13548	16943
[111]	980	Experimental values	4775	9096	10862	11979	14810
		Relative error (%)	8.7	9.8	12.4	13.1	14.4
		Computational values	5047	9862	12070	12662	15993
	1070	Experimental values	4592	8909	10738	114049	13811
		Relative error (%)	9.9	10.7	12.4	14.6	15.8

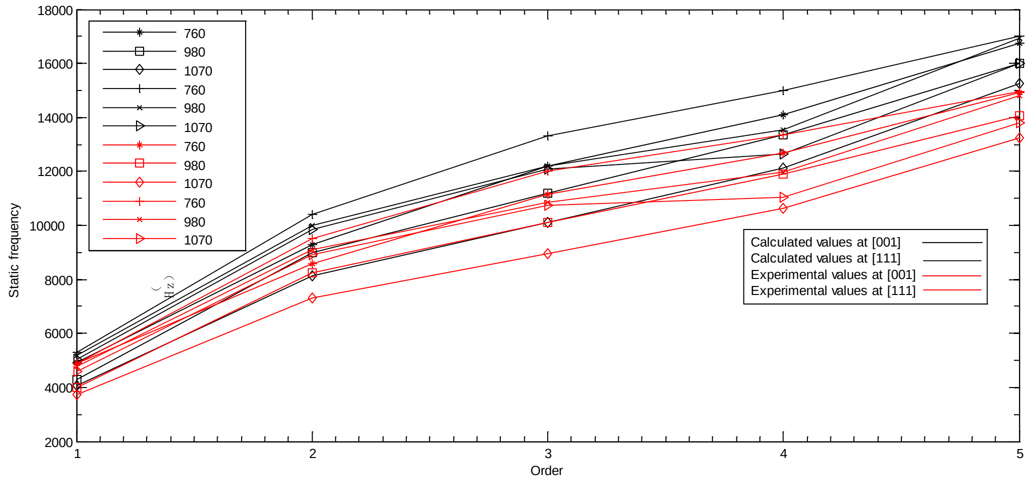

Fig. 3. Comparison of the computational and experimental results for different temperature and orientation.

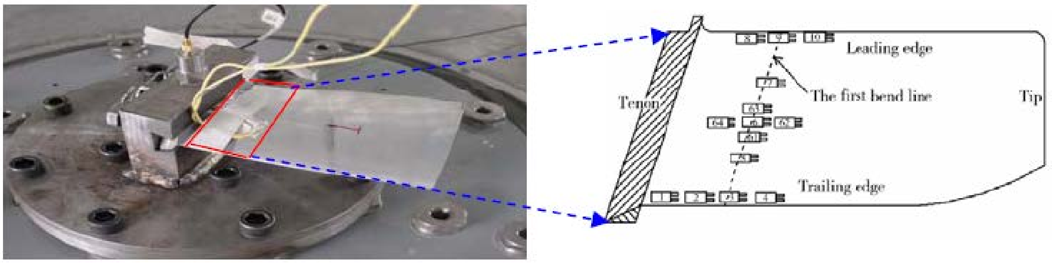

Fig. 4. Strain gage on the blade in the experiment.

different orders static frequencies were same along [001] and [111] orientations, and the orientation had stronger effect on high order static frequencies than it had on low order ones.

In order to validate the above calculated results, the vibration experiments of the DD6 alloy blade were done. According to the above discussion, the corresponding experimental results were gotten and Fig. 4 shows strain gage on the blade in the experiment.

Results showed that the maximum difference between the computational and experimental values was less than 17%, and the relative error was mainly caused by the calculated model and variable materials parameters for different temperature and orientation. Considering the theoretical model used was based on the elastic-plastic constitutive equations of a single crystal alloy, the variation of materials parameters for different temperatures and orientations could bring some influences for the calculated results. The model was used to compute the static frequencies, and the trend observation was valid by comparisons between the calculated values and the reliable experiment values in the DD6 alloy blade.

C. Residual Stresses Fields

There are four major laser parameters including the laser power density, spot size, pulse width and the number of impact. In this section, the effect on residual stresses fields with different laser power densities were investigated to analyze influence rules of residual stresses fields by single-sided LSP. Based on the above experiment, the pitch line of the first bend mode was at a distance of about 37 mm from the tenon bottom of the blade, and the tested position of vibration fatigue was focused on the neighborhood zone of the pitch line. Considering the individual difference of a DD6 blade, the shock area of DD6 blade was about at the distance of 25-60 mm from the tenon bottom to blade basic for the simulation and experiment.

Let the radius of spot size was 2.5 mm, the pulse width was 25 ns, and 50% overlapping of laser pulse was applied to the blade surface by simulation. For different laser power densities by single LSP simulation, the peak pressure of shock wave was 3, 3.5, 4 and 4.5 GPa, respectively. At last, the simulation results on the top surface and at a depth were obtained by single LSP simulation, as shown in Fig. 5. Table 2 presents the part results of calculated values on the blade surface by different laser power densities.

According to Fig. 5, the maximum compressive residual stress along the blade surface was 346 MPa when the peak pressure of shock wave was 3 GPa. The maximum compressive residual stress along the blade surface was 539 MPa when the peak pressure of shock wave was 3.5 GPa. With increasing the laser power density, the maximum compressive residual stress in the blade surface was also increased by single LSP simulation. At the same time, the corresponding LSP experiments were executed, and Fig. 6 shows the schematic principle during LSP. The residual stresses on the blade surface after LSP were measured by an X-ray stress meter. In order to improve measured precision of the stress, the swing method of four-coordinates was used to evaluate the residual stress by a type of Proto-LXRD X-ray stress meter, as shown in Fig. 7.

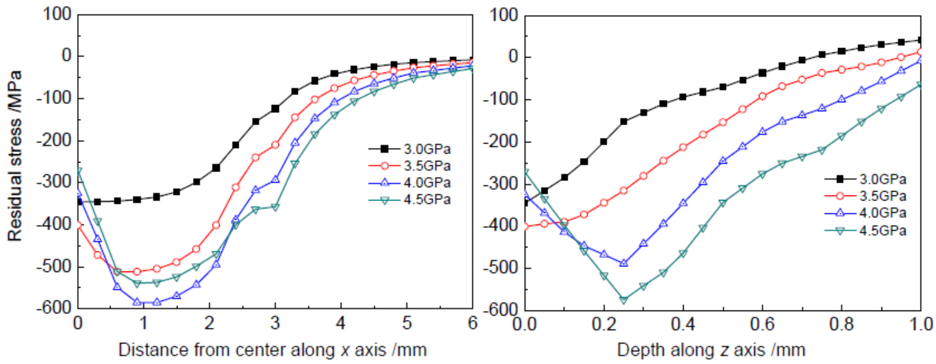

Fig. 5. Distribution curve of residual stresses.

Table 2 Part results of calculated and tested values on residual stresses along *x* axis

Item	Calculated values				Tested values			
Displacement	Power density				Power density			
along x axis/mm	3	3.5	4	4.5	3	3.5	4	4.5
0.0	-346.0	-401.0	-325.0	-271.0	-340.0	-395.0	-311.0	-260.0
0.3	-345.0	-472.0	-425.0	-391.0	-338.0	-453.0	-412.0	-376.0
0.6	-344.0	-512.0	-549.0	-511.0	-325.0	-501.0	-535.0	-495.0
0.9	-340.0	-512.0	-585.0	-539.0	-316.0	-503.0	-560.0	-517.0
1.2	-334.0	-505.0	-585.0	-537.0	-315.0	-496.0	-562.0	-523.0
1.5	-322.0	-489.0	-570.0	-524.0	-303.0	-475.0	-549.0	-515.0
1.8	-299.0	-458.0	-543.0	-499.0	-290.0	-439.0	-537.0	-476.0
2.1	-265.0	-401.0	-495.0	-469.0	-207.0	-393.0	-478.0	-452.0
2.4	-210.0	-311.0	-388.0	-400.0	-202.0	-301.0	-363.0	-388.0
2.7	-155.0	-240.0	-318.0	-363.0	-143.0	-221.0	-302.0	-346.0
3.0	-124.0	-210.0	-294.0	-357.0	-102.0	-201.0	-277.0	-331.0

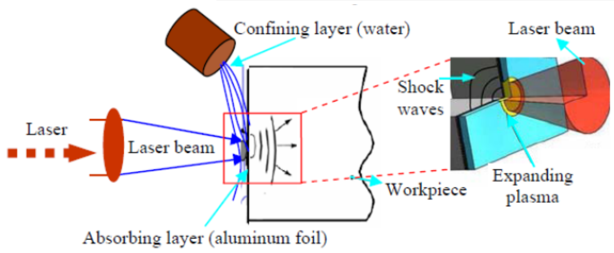

Fig. 6. Schematic principle during LSP


Fig. 7. X-ray stress meter

In the course of measuring, the swing range was ±3^o, and the angle of rotating floor was also ±3^o. After selecting some swing ranges, every value of diffraction angle was measured by the X-ray stress meter, and the measured time of every value was 30s. As a result, the residual stresses on the surface were measured by the test standard of ASTM E975-84, and the detailed measurement method could be found in literature (Fang *et al.*, 2011). Finally, the residual stresses on the blade surface were measured. Table 2 present the part results of experimental values.

According to the part values of simulation and experiment as shown in Table 2, the results indicated that harden phenomenon on the blade surface was generated with increasing the power density. It should be pointed out that proper selection of power density is of great importance for the treatment of a DD6 alloy blade in different orientation, temperature and rotor speed, which can induce a better residual stress field in the specimen to enhance the performance of the alloy blade. Namely, on the one hand, the selected laser power density should be large enough to ensure that the peak pressure of shock wave is greater than the dynamic yield strength of materials. On the other hand, the air in the LSP environment should be purified especially in order to reduce ionization of the air when selecting a high power density. Thereby, it is very important for obtaining excellent shocked effect to select suitable laser power density. By comparing the results numerical simulation with LSP experiment, a fit laser power density can be gotten according to the performance of DD6 alloy blade.

III. CONCLUSIONS

A computational model was presented to describe the dynamic properties and residual stresses induced by LSP in a certain type of DD6 blade, and the following conclusions were drawn.

(1) The finite element model established analyzes the static properties of the DD6 blade, and the maximum difference between the computational and experimental values was less than 17%. Especially, the values of stat-

ic frequency were decreased along [001] and [111] orientations with the elevated temperature, the trends of different orders static frequencies were same along [001] and [111] orientations. (2) With increasing the laser power density, simulation and experiment shown that the compressive residual stresses and plastically affected depth were extensively increased and gradually reach the saturated state. Especially, the best compressive residual stress was achieved when the power density was 4.5 GPa, found to be about 600 MPa on the blade surface. Obviously, the proposed model is far from a mature approach, and there are many work need to be improved to make it more substantial in the future work,

ACKNOWLEDGEMENTS

The authors are grateful for the support provided by the Science and Technology Plan Project of Shaanxi Province, China (grant no. 2013K07-17), the Natural Science Foundation of Shaanxi Province, China (grant no. 2012JM8004), and the National Natural Science Foundation of China (grant no. 61471387,61205002).

REFERENCES

Amarchintal, H.K., R.V. Grandhi, K. Langer and D.S. Stargel, "Material model validation for laser shock peening process simulation," *Modell. Simul. Mater. Sci. Eng.*, **17**, 1-15 (2009).

Fang, Y.W., Y.H. Li and W.F. He, "Simulation of residual stress field of diagonal laser shock processing," *Adv. Mater. Res*., **271-273**, 84-87 (2011).

Ghosh, R.N. and M. Mclean, "Modeling the orientation dependence of tertiary creep in single crystal superalloys," *Scripta Metallurgica*, **23**, 1301-1306 (1989).

Johnson, G.R, and H.C.William, "Fracture characteristics of three metals subjected to various strains, strains rates, temperatures and pressures," *Eng. Frac. Mech.*, **21**, 31-48 (1985).

He, M.H., H.Y. Li and J.X. Nie, "An investigation on creep/fatigue damage characteristics of single-crystal DD6 at high temperature," *Gas Turbine Experiment and Research*, **15**, 24-27 (2002).

Li, Y., H.C. Yu, G.D. Zhang, J.R. Li and X.R. Wu, "Effect of tensile dwell on the low fatigue behavior of DD6 nickel-based single crystal superalloy at high temperature," *Gas Turbine Experiment and Research*, **18**, 14-16 (2005).

Rubio-Gonzáleza, C., C. Felix-Martinez, G. Gomez-Rosas, J.L. Ocaña, M. Morales, J.A. Porro, "Effect of laser shock processing on fatigue crack growth of duplex stainless steel. Mater," *Mater. Sci. and Eng. A*, **528**, 914-919 (2011).

Shi, Z.X., J.R. Li, and S.Z. Liu, "High cycle fatigue behavior of the second generation single crystal superalloy DD6," *Transactions of Nonferrous Metals Society of China*, **21**, 998-1000 (2011).

Wasson, A.J., and G. E. Fuchs, "The effect of carbide morphologies on elevated temperature tensile and fatigue behavior of a modified single crystal Ni-base superalloy," *Superalloys 2008, Pennsylvania, PA, TMS*, 489-497 (2008).

Wu, B.X., S. Tao and S. Lei, "Numerical modeling of laser shock peening with femtosecond laser pulses and comparisons to experiments," *Appl. Surf. Sci.*, **256**, 4376-4382 (2010).

Zhang, Y.K., J.Z. Lu, X.D. Ren, H.B. Yao and H.X. Yao, "Effect of laser shock processing on the mechanical properties and fatigue lives of the turbojet engine blades manufactured by LY2 aluminum alloy," *Mater. Des*, **30**, 1697-1703 (2009).

Received by the Editor: November 27, 2012. Received by Subject Editor: May 15, 2014.
Accepted: February 3, 2015.
Recommended by Subject Editor: Walter Tuckart.